ICLASS-2006
Aug.27-Sept.1, 2006, Kyoto, Japan

Paper ID ICLASS06-030

TEMPERATURE MEASUREMENT IN BI-COMPONENT DROPLETS: VALIDATION OF MULTI-COMPONENT EVAPORATION MODELS

C. Maqua[1], N. Doué[2], G. Lavergne[2], F. Lemoine[1]

[1] LEMTA-CNRS UMR 7563
2, Avenue de la forêt de Haye, BP 160, 54504 Vandoeuvre-lès-Nancy, France, fabrice.lemoine@ensem.inpl-nancy.fr
[2] ONERA/DMAE
[2]ONERA-DMAE Toulouse Center, 2 avenue Edouard Belin - BP 4025
31055 Toulouse cedex, France, gerard.lavergne@onecert.fr

ABSTRACT The optimization of the combustion process of liquid commercial petroleum requires the fine understanding of multi-component droplet vaporization, especially when each component evaporates at different boiling temperatures.
This paper presents the application of a novel technique to the study of the temperature of bi-component droplets along a monodisperse stream. Based on the three-color extension of the two-color laser-induced fluorescence (LIF) technique, mean droplet temperatures can be measured regardless of the composition. The method requires adding a fluorescent organic dye at low concentration to a fuel composed with a mixture of ethyl-alcohol and acetone. The ratio between the fluorescence signals collected on two spectral bands (having different temperature sensitivities) is then a function of the temperature, regardless of laser intensity, time-dependent tracer concentration, and measurement volume. The approximate overall accuracy is then of $\pm$ 1.3°C. The technique is demonstrated on monodisperse droplets injected in a hot air plume. An extensive study of the influence of the fuel initial composition and droplet diameter is performed. Finally, the experimental data are compared to the results of a numerical simulation based on the discrete components model.

KEYWORDS: multicomponent droplets, laser-induced fluorescence, temperature, evaporation, ethanol, acetone

1. INTRODUCTION

The problem of heat and mass transfer between a dispersed phase and a gas phase is encountered in numerous industrial processes and particularly in the spray combustion field. Most power producing combustion devices employ sprays of commercial petroleum fuels. A better knowledge of multi-component droplet vaporization and combustion processes inside sprays is required. In this field, the understanding of the time dependent evaporation mechanisms of multicomponent droplets is essential, especially when each component evaporates at different boiling temperatures. Indeed, fuel composition significantly influences local fuel-air ratio, and therefore, ignition delays and pollutant emissions. Although dropletsize can be easily measured, temperature measurements are still a challenge, even for monocomponent droplets. Experimental investigations require having diagnostics, which are able to measure the droplet temperature. Optical diagnostics applied to multicomponent droplets are rare and only light scattering based techniques are reported in the literature. Applications of rainbow refractometry have been mentioned by Zhao and Qiu [1] and Wilms et al. [2].
This paper presents the application of a novel technique, based on the three-color laser-induced fluorescence [3], to the study of the temperature of bi-component droplets along a monodisperse stream. The technique has been tested on binary droplets (about 100 to 200 µm in diameter) composed of mixtures of acetone and ethyl-alcohol (ethanol), streaming linearly. The droplet stream was injected inside a hot air plume. Different compositions and two droplets diameters are then studied. In parallel, a numerical simulation based on the 1D approach has been implemented using the discrete component model [4]. The finite conduction of the liquid phase, as well as the influence of within droplet fluid circulation is taken into account.

2. THREE COLOR LASER-INDUCED FLUORESCENCE PRINCIPLES

2.1. Application to monocomponent droplets: two color laser-induced fluorescence

The liquid is seeded with a low concentration (a few mg/l) of rhodamine B before being disintegrated into droplets. Rhodamine B is an organic dye, used as a fluorescent temperature sensor. Furthermore, the fluorescence of rhodamine B can easily be induced by the green line of the argon ion laser (λ = 514.5 nm). The fluorescence intensity, collected on a spectral band $[\lambda_{i1};\lambda_{i2}]$, i denoting the spectral band, is given by [5]:

$$I_{fi} = \int_{\lambda_{i1}}^{\lambda_{i2}} K_{opt}(\lambda) K_{spec}(\lambda) V_C I_0 C e^{\beta(\lambda)/T} d\lambda \approx K_{opt,i} K_{spec,i} V_C I_0 C e^{\beta_i/T} \quad (1)$$

where $K_{opt,i}$ is an optical constant taking into account the properties of the detection system (e.g. solid angle of detection and transmission of the optical components),

$K_{spec,i}$ is a constant depending solely on the spectroscopic properties of the fluorescent tracer in its solvent, both for the spectral band *i*. I_0 is the laser excitation intensity, C is the molecular tracer concentration, T is the absolute temperature, and V_c is the volume where the fluorescence photons are collected. In fact this volume is the intersection between the laser beams, the droplet volume and the volume defined by the collecting optics. The product $C.V_c$ is related to the number of fluorescence photons collected by the photodetector. The factor $\beta(\lambda)$ characterizes the temperature dependence of the fluorescence intensity at the wavelength λ [3] and β_i characterizes the temperature dependence of the fluorescence emitted on the spectral band *i*. To properly measure the temperature of a moving and potentially evaporating droplet, the influence of the parameters $C.V_c$ and I_0 must be removed. The collection volume V_c is constantly changing as the droplet crosses the probe volume. Furthermore, the distribution of the laser intensity within the droplet depends on the relative position of the droplet and also on the laser beam shape, which is influenced by the refractive and focusing effects of the droplet surface. To eliminate these issues, the fluorescence intensity is detected on two spectral bands for which the temperature sensitivity is strongly different. The ratio of the fluorescence intensities collected on both optimized spectral bands is given by:

$$R_{12} = \frac{I_{f_1}}{I_{f_2}} = \frac{K_{opt,1}}{K_{opt,2}} \frac{K_{spec,1}}{K_{spec,2}} e^{\frac{\beta_1 - \beta_2}{T}} \qquad (2)$$

This ratio is independent on the dimensions of the probe volume. The influence of the local laser intensity and the tracer concentration are eliminated as well. The use of a single reference measurement at a known temperature allows eliminating the optical and spectroscopic constants.

2.2. Application to binary droplets: three color laser-induced fluorescence

In the present study, mixtures of acetone and ethanol will be considered and the ethanol volume fraction in the mixture will be denoted by χ. Preliminary spectroscopic studies have shown that the fluorescence spectrum of rhodamine B in a solvent depends on both temperature and solvent composition ([3] et [6]). The factor β_i describing the influence of temperature on fluorescence intensity is also likely to depend on the solvent composition. In case of binary fuels, a function $\gamma(\lambda,\chi)$, depending also on the fluorescence emission wavelength λ, must be added in order to take into account the influence of the mixture composition on the fluorescence intensity.

The new expression of the fluorescence intensity integrated on a given spectral band *i* is:

$$\begin{aligned} &\int_{\lambda_{i1}}^{\lambda_{i2}} K_{opt}(\lambda) K_{spec}(\lambda) V_C I_0 C \gamma(\lambda,\chi) e^{\frac{\beta(\lambda,\chi)}{T}} d\lambda \\ &\approx K_{opt,i} K_{spec,i} V_C I_0 C \gamma_i(\chi) e^{\frac{\beta_i(\chi)}{T}} \quad (i=1,2) \end{aligned} \qquad (3)$$

where $\gamma_i(\chi)$ is a function taking into account the influence of the mixture fraction on the fluorescence emission for the spectral band *i*.

To determine properly the temperature of such binary droplets, an additional equation will be necessary, since a dependence on the ethanol volume fraction χ has been added. The signal should be detected on a third spectral band, for which the sensitivity on the temperature T and ethanol volume fraction χ is different from the two other one. The fluorescence intensity on the third spectral band can be simply expressed using Eq. (3), with *i*=3.

Using Eq. (3), two fluorescence ratios can be calculated:

$$\begin{aligned} &R_{ij} = \frac{I_{f_i}}{I_{f_j}} = \frac{K_{opt,i}}{K_{opt,j}} \frac{K_{spec,i}}{K_{spec,j}} \frac{\gamma_i(\chi)}{\gamma_j(\chi)} e^{\frac{\beta_{ij}(\chi)}{T}} \\ &(i,j) = \{(1,2),(2,3)\} \end{aligned} \qquad (4)$$

where β_{ij} denotes $\beta_i - \beta_j$.

In order to optimize the selection of the three spectral bands, a preliminary spectroscopic study has been performed: fluorescence spectra have been recorded for several ethanol volume fractions and for a range of liquid temperatures. A trade-off between crossed temperature and composition sensitivities and signal level leads to the following selection of the three spectral bands:

- Band 1: [525 nm ; 535 nm]
- Band 2: [535 nm ; 545 nm]
- Band 3: [570 nm ; 700 nm]

3. CALIBRATION AND MEASUREMENT PROCESS

3.1. Optical set-up

A Laser Doppler Anemometry (LDA) laser beams system is used to generate the probe volume, which allows measuring the droplet velocity concomitantly, with the use of an additional Doppler signal processor. The probe volume formed by the intersection of the laser beams, is 1200 µm long and is 150 µm in diameter (transverse direction). The fluorescence signal is detected by an achromatic doublet, located at right angle, connected to an optical fiber acting as a pinhole. The laser light (λ = 514.5 nm) scattered by the droplets is high-pass filtered with the use of a notch filter in order to collect only the fluorescence emission. The remaining fluorescence signal is separated into the three spectral bands by means of a set of neutral beamsplitters and interference filters (figure 1). The optical signal detection on the selected three spectral bands is performed by means of three cooled photomultipliers. The acquisition, digitization and sampling of the fluorescence signals are carried out by means of a rapid computerized multi-channel acquisition board, with a sampling rate of 5 MHz.

3.2. Initial calibrations

All the calibration experiments are performed in an agitated temperature controlled quartz-made cell (figure 1). The functions $\beta_{12}(\chi)$ and $\beta_{23}(\chi)$ are determined using the equation set (4). For a given ethanol volume

fraction χ, the quantities $\ln\left(R_{ij}(T,\chi)/R_{ij}(T_0,\chi)\right)$ $(i,j)=\{(1,2),(2,3)\}$ are represented as a function of $(1/T-1/T_0)$ (figure 2). The reference temperature T_0 allows normalizing the fluorescence ratios and then eliminating the optical and spectroscopic constants. As expected, the functions $\beta_{12}(\chi)$ and $\beta_{23}(\chi)$ present a clear dependence on χ (figure 3); these behaviours can be fitted by polynomial approximations.

The fluorescence ratios $R_{12}(T,\chi)$ and $R_{23}(T,\chi)$ (Eq. (4)) are normalized by $R_{12}(T,\chi_0)$ and $R_{23}(T,\chi_0)$ respectively, where χ_0 is a reference ethanol volume fraction, in order to determine the function $\gamma(\chi)$. The functions $\beta_{12}(\chi)$ and $\beta_{23}(\chi)$ being known by the previous experiments, two new functions $f_{12}(\chi)$ and $f_{23}(\chi)$ can be defined:

$$f_{ij}=\frac{\gamma_i(\chi)}{\gamma_i(\chi_0)}\frac{\gamma_j(\chi_0)}{\gamma_j(\chi)}=\frac{R_{ij}(T,\chi)}{R_{ij}(T,\chi_0)}e^{-\frac{\beta_{ij}(\chi)-\beta_{ij}(\chi_0)}{T}} \quad (5)$$
$$(i,j)=\{(1,2),(2,3)\}$$

The functions $f_{12}(\chi)$ and $f_{23}(\chi)$ are plotted also in figure 3 where a clear monotonous trend is observale as well. Polynomial fits are also used to describe the behavior of $f_{12}(\chi)$ and $f_{23}(\chi)$.

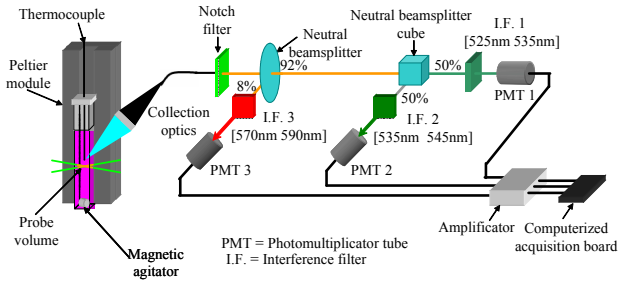

Figure 1: Optical arrangement implemented for the calibration experiments.

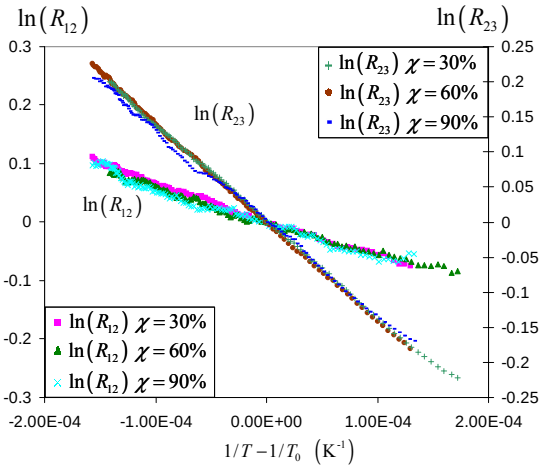

Figure 2: Temperature calibration of the functions β.

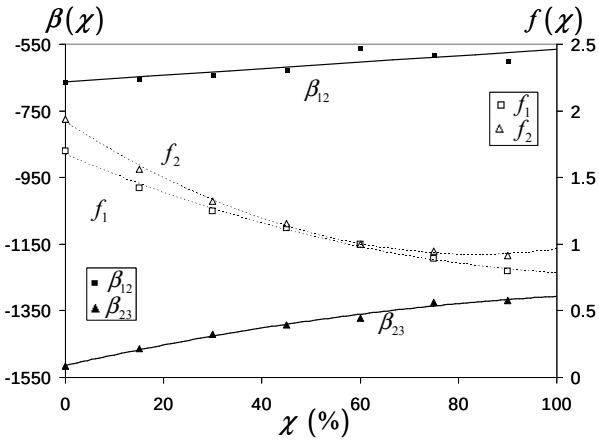

Figure 3: Calibration of the functions β and f as a function of the ethanol volume fraction.

3.3. Droplet temperature determination

The injection conditions, such as the temperature T_{inj} and ethanol volume fraction χ_{inj} are fixed in first. The reference conditions used for eliminating K_{opt} and K_{spec} are taken at the injection point. Using the equation set (4), the normalized fluorescence ratios can be written:

$$\ln\left(R_{ij}/R_{ij,inj}\right)=\ln\left(f_{ij}(\chi)/f_{ij}(\chi_{inj})\right)$$
$$+\beta_{ij}(\chi)/T-\beta_{ij}(\chi)/T_{inj} \qquad (i,j)=\{(1,2),(2,3)\} \quad (6)$$

where $R_{ij,inj}$ are the reference fluorescence ratios at the injection point. Since the functions $f_{12}(\chi)$, $f_{23}(\chi)$, $\beta_{12}(\chi)$ and $\beta_{23}(\chi)$ have been determined previously, the equation set (6) can be resolved in order to derive the temperature T and the ethanol volume fraction χ.

The different uncertainties on the calibration process and on the measurement itself lead to an overall approximate accuracy of $\pm 1.3°C$ on temperature and $\pm 4\%$ on ethanol volume fraction.

4. EXPERIMENTAL FACILITIES

4.1. Experimental set-up

A monodisperse droplet stream is generated by disintegration of a liquid jet by a piezoceramic [7]. The fuel can be pre-heated in the injector body and the temperature can be measured accurately just before the injection point by means of a K type thermocouple. The monodisperse droplets are injected in a hot air co-flowing stream, issuing from two electrical heaters, arranged symmetrically according to the droplet streaming axis (figure 4). The hot air velocity in the vicinity of the droplet stream injection point is about 2 m/s. The hot air stream temperature field, serving as boundary conditions for the droplets, was previously characterized by a thermocouple: the air temperature evolves from 550°C at the injection point to about 100°C at y=60 mm (figure 5). Downstream distance from the injection point can be easily converted into

time by using the local droplet velocity measured by laser Doppler anemometry.

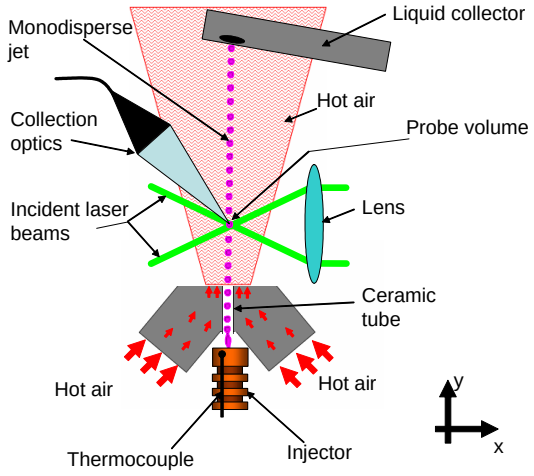

Figure 4: Experimental arrangement of droplet injection in the hot air plume.

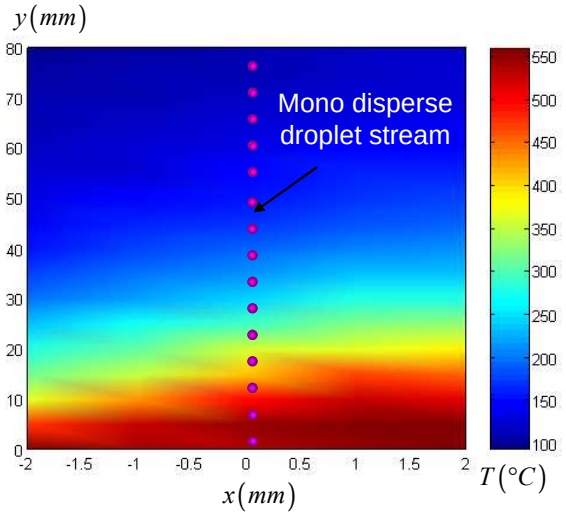

Figure 5: Temperature field in the hot air plume.

5. PHYSICAL MODELING AND SIMULATIONS

The usual assumptions are considered: spherically symmetric system, quasi-steady gas phase and variable physical properties. The liquid composition is represented by the discrete components model developed by Sirignano [4], which consider each individual species. The species and temperature within the droplets are given by resolving the following equations taking into account the effect of the internal liquid circulation:

$$\frac{\partial Y}{\partial t}-\frac{r^*}{R}\frac{dR}{dt}\frac{\partial Y}{\partial r^*}+\frac{1}{R}\vec{v}.\overrightarrow{\nabla_{r^*}}Y=\frac{D_l}{R^2}\Delta_{r^*}Y \qquad (7)$$

$$\frac{\partial T}{\partial t}-\frac{r^*}{R}\frac{dR}{dt}\frac{\partial T}{\partial r^*}+\frac{1}{R}\vec{v}.\overrightarrow{\nabla_{r^*}}T=\frac{a}{R^2}\Delta_{r^*}T \qquad (8)$$

where $r^*=\frac{r}{R(t)}$.

It will be assumed that the internal streamlines of the liquid circulating within the droplet follows a spherical Hill vortex pattern, according to stream function ψ [8]:

$$\psi\left(r^*,\theta,\varphi\right)=-\frac{U_s R^2}{2}r^{*2}\left(1-r^{*2}\right)\sin^2\theta \qquad (9)$$

where $\left(r^*,\theta,\varphi\right)$ are the spherical coordinates of a point within the droplet. According to Sirignano [9], this flow pattern should remain still valid in the case of interacting droplets, only the drag coefficient, heat and mass transfer numbers are likely to be modified.

As a consequence of Eq. (9), the maximum surface velocity U_S may be estimated as $U_S=\frac{1}{6\pi}\left(V_\infty-V\right)\left(\frac{\mu_g}{\mu_l}\right)\mathrm{Re}\,C_F$ [9]. The friction coefficient C_F suggested in [9], in the case of an isolated evaporating droplet, is $C_F=\frac{12.69}{\mathrm{Re}^{2/3}\left(1+B_M\right)}$. The parameter B_M is the Spadling mass transfer number, defined by $B_M=\frac{Y_{ethv,s}+Y_{acev,s}-Y_{ethv,\infty}-Y_{acev,\infty}}{1-Y_{ethv,s}-Y_{acev,s}}$ in the case of binary droplets. The physical properties of the gas phase are evaluated at the reference state (T_{ref} and Y_{ref}) according to the "1/3 rule" [10]:

$T_{ref}=T_S+\left(T_{amb}-T_S\right)/3$

and $Y_{k,ref}=Y_{k,S}+\left(Y_{k,amb}-Y_{k,S}\right)/3$ (10)

The fuel vapor fraction $Y_{i,S}$ is determined, assuming the liquid-vapor equilibrium, by the Clausius-Clapeyron law [11] and the Raoult law is applied at the droplet surface:

$$X_{kvs}=X_{kls}\frac{P_{sat}\left(T\right)}{Pa} \qquad (11)$$

Eqs. (7) and (8) are solved under initial condition $T(r,t=0)=T_{inj}$ and $Y_k(r,t=0)=Y_{k,inj}$ supplemented by the conditions at the droplet surface $2\pi R^2\lambda_l\int_{\theta=0}^{\pi}\left(\frac{\partial T}{\partial r}\right)_{r=R}\sin\theta\,d\theta=Q_L(t)$ and

$\dot{m}_k=\dot{m}Y_{k,ls}-2\pi R^2\rho_l D_{k,l}\int\left.\frac{d\left(Y_{k,l}\right)}{dr}\right|_{r=r_S}\sin(\theta)d\theta$, where Q_L is the heat flux penetrating into the droplet by conduction and convection from the gas phase and $\dot{m}_k$ is the mass flux of the specie k.

The instantaneous heat flux Q_L is evaluated by means of the overall energy budget equation, neglecting the radiative exchanges:

$$Q_L=\Phi_C-\Phi_{vap} \qquad (12)$$

where $\Phi_C=\dot{m}\frac{Cp_v\left(T_\infty-T_S\right)}{B_T}$ is the convective heat flux exchanged with the gaseous environment and $\Phi_{vap}=L_{veth}\dot{m}_{eth}+L_{vace}\dot{m}_{ace}$ is the heat flux due to vaporization. B_T is the Spalding thermal transfer number defined by:

$$B_T = \frac{\dot{m} C_{pg} \left(T_{amb} - T_s \right)}{L_{veth} \dot{m}_{eth} + L_{vace} \dot{m}_{ace}} \quad (13)$$

The instantaneous total mass flux $\dot{m}$ is given by $\dot{m} = \pi D \rho_g Sh_k \ln\left(1 + B_{Mk}\right)$, where B_{Mk} is the Spalding mass transfer number for the component k defined by:

$$B_{Mk} = \frac{Y_{k,s} - Y_{k,\infty}}{\frac{\dot{m}_k}{\dot{m}} - Y_{k,s}} \quad (14)$$

The Sherwood number Sh follows the expression suggested in [9]. In such a configuration, the influence of the droplet to droplet interactions should be taken into account, since the reduced distance parameter C is on the order of a few units. It is known that the decrease of the droplet spacing leads to a decrease of the Nusselt and Sherwood numbers [11]. Therefore, the effects of the interaction on Sherwood number may be described by applying a reduction factor $\eta(C)$, depending only on the reduced droplet spacing C [11]. The correlation suggested in. [12], for $2.5 \le C \le 16$, obtained in the case of evaporating monodsiperse droplets in linear stream, was used:

$$\eta(C) = \frac{Sh}{Sh_{iso}} = 1 - 0.57\left(1 - \frac{1 - 0.57e^{-0.13(C-6)}}{1 + 0.57e^{-0.13(C-6)}}\right) \quad (15)$$

where Sh_{iso} represents the Sherwood number for an isolated moving evaporating droplet [9]. The resolution of Eqs. (7) and (8) is performed by splitting the dimensionless temperature on the Legendre polynomials base [13].

6. EXPERIMENTAL RESULTS, COMPARISON TO NUMERICAL SIMULATIONS

The droplets are injected in the hot air plume, already described in section 4.1. Different ethanol volume fractions were tested: χ_{inj} = 0 (pure acetone), χ_{inj} = 25%, 75% and χ_{inj} =100% (pure ethanol), for two different droplet sizes (D_{inj}= 130 µm and D_{inj}= 230 µm). The fuel injection temperature is adjusted so as to obtain the same droplet temperature at the position where the droplet are injected in the hot air plume (y=0, figure 4). The droplets are injected at a velocity of about 9.5 m/s, which decreases downstream due to the drag force effects. The droplet temperature is measured at different downstream positions and its evolution as a function of time is presented in figure 6 for D_{inj}= 130 µm and figure 7 for D_{inj}= 230 µm. In the initial zone of the hot air plume, the droplets are heated due to the predominance of the heat transfers by forced convection from the gas phase. Then, when the air temperature is lower, evaporation phenomena become dominant and the droplet temperature decreases. Regardless to the droplet size, a noticeable influence of the composition of the mixture on the droplet temperature evolution is observed. It can be noticed that the initial heating of the droplets is all the more important that the initial fraction of the less volatile component (i.e. ethanol) is high. The increase in the fraction of the more volatile component, i.e. acetone, contributes noticeably to increase the heat flux extracted by evaporation, since the acetone saturated pressure is 3.7 times these of ethanol in this range of temperature. Then, following the initial heating phase, the observed droplet cooling is stronger.

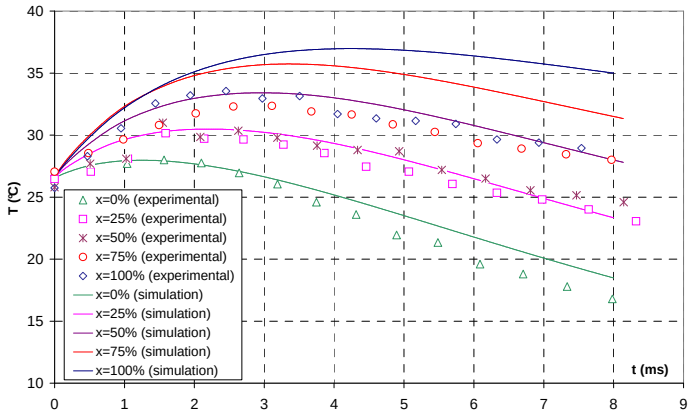

Figure 6: Droplet temperature evolution in the hot air plume and comparison to the numerical simulation (D_{inj}=130 µm).

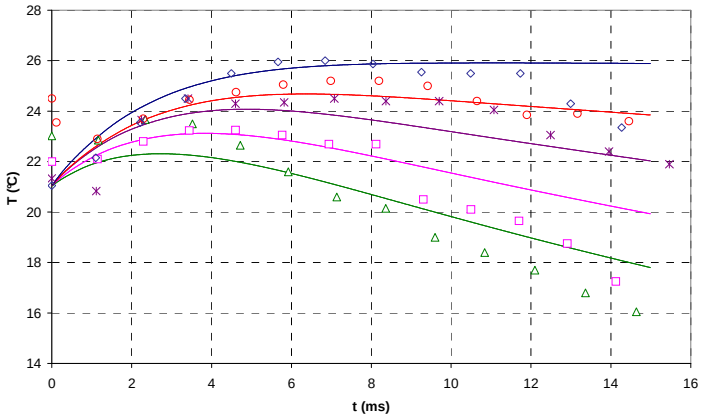

Figure 7: Droplet temperature evolution in the hot air plume and comparison to the numerical simulation (D_{inj}=230 µm) (same caption like in figure 6).

Although the general trend is similar for the droplets of highest diameter (230 µm), the droplet temperature evolves in a smaller range, because the biggest droplets have a smaller ratio between the surface of exchange and volume.

A numerical simulation is performed using the principles and models described in section 5. A map of temperature and ethanol volume fraction within the droplet is presented in figure 8. It is clear that the mass diffusion is more influenced by the internal fluid circulation than heat.

Generally, the numerical data follows a trend similar to the experimental results, i.e. a heating phase followed by a temperature decrease caused by the strong vaporization. For the smallest droplets (D=130 µm, figure 6), a reasonable agreement is found for pure acetone and for the smallest fraction of ethanol (χ=25%). The agreement between experimental and numerical results is deteriorating for ethanol fractions higher than 25%. The bad agreement for high ethanol volume fractions may be attributed to an inadequate calculation of the physical properties in the gas phase, at the reference state, determined according to the usual empirical "1/3 rule". Parameters such as gaseous ethanol (or acetone) diffusivity in the vapor mixture are very sensitive to temperature and can strongly influence the numerical simulation results.

The situation seems better for the biggest droplets (D=230 µm, figure 7), because the heat capacity of the droplets is much more important and the vaporization rate, which is strongly dependent on the gas phase physical properties, has less influence.

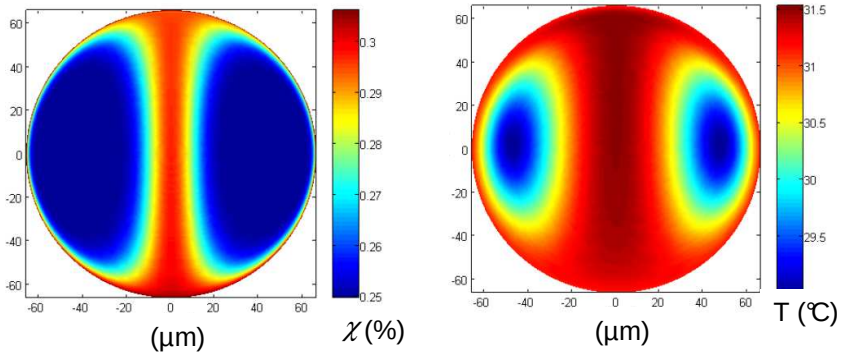

Figure 8: Map of temperature and ethanol volume fraction within the droplet at t=2.1 ms (130 µm droplet).

7. CONCLUSIONS

The transient temperature of moving evaporating binary droplets has been measured by a new laser-induced fluorescence technique, based on the detection of the fluorescence emission of a temperature sensitive dye on three spectral bands. The effect of composition and temperature variations on the fluorescence emission can be clearly separated and the temperature can be inferred within ±1.3°C. Experiments consisting in injecting monodisperse droplets in linear stream into a coflowing hot air plume. The experimental data were compared to numerical simulations based on the discrete component model: the observed discrepancies, especially for the high ethanol volume fractions, can be probably be

explained by an inadequate determination of the physical properties and potentially of the reference state. Further investigations will concentrate on this point.

NOMENCLATURE

a	thermal diffusivity
B_M	Spalding mass transfer number
B_T	Spalding heat transfer number
C_p	Specific heat capacity
C=L/D	non-dimensional distance parameter
D	droplet diameter
$D_{l,g}$	molecular diffusivity (liquid or gas)
L	droplet spacing
L_v	latent heat of vaporization
R	droplet radius
Re	droplet Reynolds number
Sh	Sherwood number
T	temperature
U_s	maximum velocity at the droplet surface
V	velocity
V_∞	free stream velocity
X	molar fraction
Y	mass fraction

Greek symbols

μ	dynamic viscosity
λ	thermal conductivity
χ	ethanol volume fraction
ρ	specific density
ψ	stream function

Subscript:

ace	acetone
amb	ambient conditions
eth	ethanol
g	gas phase
i	spectral band index
k	k^{th} component of the fuel
inj	injection
l	liquid phase
ref	reference
s	droplet surface

Acknowledgement: This program has been conducted in the framework of the ASTRA program, supported by CNRS and ONERA.

REFERENCES

1. Zhao Y., Qiu H.H., Measurements of multicomponent microdroplet evaporation by using rainbow refractometer and PDA, Exp. in Fluids, vol. 40, pp 60-63, 2006.
2. Wilms J., Roth N., Arndt S., Weigand B., Determination of the composition of multicomponent droplets by rainbow refractometry, 12th Symposium on Application of Laser Techniques to Fluid Mechanics, Lisbon, Portugal, 2004.
3. Lavieille P., Lemoine F., Lavergne G., Lebouché M., Evaporating and combusting droplet temperature measurements using two-color laser-induced fluorescence, Exp. in Fluids, vol. 31, pp. 45-55, 2001.
4. Sirignano W.A., Fluid dynamics and transport of droplets and sprays, Cambridge University Press, 1999.
5. Castanet G., Lavieille P., Lebouché M., Lemoine F., Measurement of the temperature distribution within monodisperse combusting droplets in linear stream using two colors laser-induced fluorescence, Exp. in Fluids, vol. 35, pp. 563-571, 2003.
6. Lavieille P., Delconte A., Blondel D., Lebouché M., Lemoine F., Non-Intrusive temperature measurements using three-color laser-induced fluorescence, Exp. in Fluids, vol. 36, pp. 706-716, 2004.
7. Lavieille P., Lemoine F., Lebouché M., Experimental investigation on interacting low evaporating droplets temperature in linear stream using two colors laser induced fluorescence, Comb. Sci. Tech., vol. 174 (4), pp 117-142, 2002.
8. Clift R., Grace J.R., Weber M.E., Bubbles, drops, and particles. Academic, New York, 1978.
9. Abramzon B., Sirignano W.A., Droplet vaporization model for spray combustion calculations, International Journal of Heat and Mass Transfer, vol. 32, pp. 1605-1618, 1989.
10. Hubbard G.L., Denny V.E., Mills A.F., Droplet evaporation: effects of transient and variable properties, International Journal of Heat and Mass Transfer, vol. 18, pp. 1003-1008, 1975.
11. Castanet G., Lebouché M., Lemoine F., 2005, Heat and mass transfer of combusting monodisperse droplets in linear stream, International Journal of Heat and Mass Transfer, vol. 48, pp. 3261-3275, 2005.
12. Atthasit A., Doué N., Biscos Y., Lavergne G., Influence of droplet concentration on the dynamics and evaporation of a monodisperse stream of droplets in evaporation regime, Advances in Combustion and Atmospheric Pollution, Semenov Memorial, Russia, Torus Press, pp. 19-36, 2005.
13. Castanet G., Lavieille P., Lebouché M., Lemoine F., Experimental and theoretical investigation of the heating of combusting droplets in linear stream, Comb. Sci. Tech., vol. 177, pp. 2395-2422, 2000.